Coherent response of Antarctic Intermediate Water and Atlantic Meridional Overturning Circulation during the last deglaciation: reconciling contrasting neodymium isotope reconstructions from the tropical Atlantic

Sifan Gu[a,*], Zhengyu Liu[a,*], Jiaxu Zhang[a], Johannes Rempfer[b], Fortunat Joos[b], Delia W. Oppo[c]

[a]Department of Atmospheric and Oceanic Sciences and Center for Climatic Research, University of Wisconsin-Madison, Madison, WI, USA;

[b]Climate and Environmental Physics, Physics Institute and Oeschger Center for Climate Change Research, University of Bern, Bern, Switzerland

[c]Department of Geology and Geophysics, Woods Hole Oceanographic Institution, Woods Hole, MA, USA

Corresponding author: Sifan Gu (sgu28@wisc.edu) and Zhengyu Liu (zliu3@wisc.edu)

Key Points:

- Antarctic Intermediate Water northward penetration is controlled by the Atlantic Meridional Overturning Circulation strength.
- Atlantic Intermediate Water becomes deeper and thicker during weaker Atlantic Meridional Overturning Circulation period.
- The contradictory ε_{Nd} reconstructions from the tropical Atlantic are due to the site location and depth and the influence of different water masses.

Abstract

Antarctic Intermediate Water (AAIW) plays important roles in the global climate system and the global ocean nutrient and carbon cycles. However, it is unclear how AAIW responds to global climate changes. In particular, neodymium isotopic composition (ε_{Nd}) reconstructions from different locations from the tropical Atlantic, have led to a debate on the relationship between northward penetration of AAIW into the tropical Atlantic and the Atlantic Meridional Overturning Circulation (AMOC) variability during the last deglaciation. We resolve this controversy by studying the transient oceanic evolution during the last deglaciation using a neodymium-enabled ocean model. Our results suggest a coherent response of AAIW and AMOC: when AMOC weakens, the northward penetration and transport of AAIW decreases while its depth and thickness increase. Our study highlights that as part of the return flow of the North Atlantic Deep Water (NADW), the northward penetration of AAIW in the Atlantic is determined predominately by AMOC intensity. Moreover, the inconsistency among different tropical Atlantic ε_{Nd} reconstructions is reconciled by considering their corresponding core locations and depths, which were influenced by different water masses and ocean currents in the past. The very radiogenic water from the bottom of the Gulf of Mexico and the Caribbean Sea, which was previously overlooked in the interpretations of deglacial ε_{Nd} variability, can be transported to shallow layers during active AMOC, and modulates ε_{Nd} in the tropical Atlantic. Changes in the AAIW core depth must also be considered. Thus, interpretation of ε_{Nd} reconstructions from the tropical Atlantic is more complicated than suggested in previous studies.

1 Introduction

Antarctic Intermediate Water (AAIW) is a key component of the global ocean circulation. Large volume northward flowing AAIW plays an important role in the northward nutrient transport to sustain primary production in the North Atlantic [*Sarmiento et al.*, 2004; *Palter and Lozier*, 2008]. It also contributes to the anthropogenic carbon sink [*Sabine*, 2004; *Gruber et al.*, 2009] and the ocean acidification [*Ito et al.*, 2010; *Resplandy et al.*, 2013]. However, how AAIW responds to global climate changes has remained poorly understood. In particular, how AAIW interacts with the Atlantic Meridional Overturning Circulation (AMOC) remains highly controversial. The last deglaciation presents an ideal target to test our understanding of the relation between AAIW and AMOC. Some previous observational studies of the last deglaciation suggested that the northward penetration of AAIW in the tropical Atlantic should be positively correlated with the AMOC strength [*Came et al.*, 2008; *Xie et al.*, 2012; *Huang et al.*, 2014]. This positive correlation seems to be consistent with the notion that AAIW, as part of the North Brazil Current (NBC), contributes to the return branch of North Atlantic Deep Water (NADW) [*Rintoul*, 1991; *Schmitz and McCartney*, 1993; *Lumpkin and Speer*, 2003; *Zhang et al.*, 2011]. However, other observational studies infer an enhanced AAIW penetration into the tropical Atlantic with a collapsed AMOC during the last deglaciation, or a negative correlation between the AAIW penetration and AMOC intensity [*Zahn and Stüber*, 2002; *Rickaby and Elderfield*, 2005; *Pahnke et al.*, 2008]. This negative correlation appears to be consistent with some other modeling studies, which simulate an increased AAIW transport into the North Atlantic in a counterclockwise shallow AAIW cell after the initial collapse of AMOC [*Saenko et al.*, 2003; *Weaver et al.*, 2003; *Stouffer et al.*, 2007]. The different relationship between AAIW northward penetration in the Atlantic and the AMOC strength suggests different roles of AAIW in AMOC: a positive correlation implies the AAIW penetration as a subsequent response to the AMOC reorganization while a negative correlation indicates that the AAIW penetration may provide a positive feedback or a trigger for AMOC reorganization as more fresh water is transported to the North Atlantic by AAIW when AMOC is weaker [*Pahnke et al.*, 2008]. In addition, understanding the relationship between the AAIW northward penetration in the Atlantic and AMOC also helps to understand the mechanisms of nutrient supply change in low latitude Atlantic across the deglaciation, which is also under debate [*Meckler et al.*, 2013; *Hendry et al.*, 2016].

In studying the AAIW evolution during the last deglaciation, we will pay particular attention to neodymium (Nd) isotopic composition (ε_{Nd}), which has emerged as a promising quasi-conservative tracer for water masses [*Goldstein and Hemming*, 2003]. ε_{Nd} is defined as $[(^{143}Nd/^{144}Nd)_{sample}/(^{143}Nd/^{144}Nd)_{CHUR} - 1]*10^4$, where $(^{143}Nd/^{144}Nd)_{CHUR}$ is 0.512638, which is the bulk earth composition defined by the Chondritic Uniform Reservoir [*Jacobsen and Wasserburg*, 1980]. The ε_{Nd} exhibits distinct values geographically, with the most radiogenic (highest) values in the North Pacific (0~-5), intermediate values in the Southern Ocean and the Indian Ocean (-7~-10) and the least radiogenic (lowest) values in the North Atlantic (-10~-14). This strong ε_{Nd} gradient has motivated using ε_{Nd} as a tracer for Northern versus Southern water mass mixing. Unlike tracers such as $\delta^{13}C$ and Cd/Ca, which are highly influenced by biological processes in addition to ocean circulation, biological or chemical fractionation of ε_{Nd} is negligible [*Goldstein and Hemming*, 2003]. Furthermore, ε_{Nd} is relatively insensitive to potential Nd source changes as unrealistically extreme changes in Nd sources are required in the model to produce the magnitude of ε_{Nd} changes comparable to reconstructions [*Rempfer et al.*, 2012b]. Variations of ε_{Nd} is able to reflect the strength of overturning circulation in idealized fresh water hosing experiments [*Rempfer et al.*, 2012a]. Therefore, ε_{Nd} appears to be an effective tracer for water masses and has been increasingly used in paleoceanographic studies.

In the tropical Atlantic, a more radiogenic ε_{Nd} at the AAIW depth would imply a stronger AAIW influence (from the Southern Ocean) with an enhanced AAIW northward penetration, and vice versa, if the end-member ε_{Nd} values are stable. Although the North Atlantic water mass ε_{Nd} end-member is complicated by NADW source waters, which are distinct in ε_{Nd} [*van de Flierdt et al.*, 2016], end-member ε_{Nd} of northern-sourced water is suggested to be stable on glacial-interglaical to millennial timescales [*van de Flierdt et al.*, 2006; *Foster et al.*, 2007]. ε_{Nd} from the southern Brazil margin at intermediate depth also shows no changes across the last deglaciation [*Howe et al.*, 2016]. Furthermore, a modeling study [*Rempfer et al.*, 2012a] suggests that effect of end-member ε_{Nd} changes are much smaller than the effect of changes in water mass distribution on the millennial time scale.

The controversy on the relationship between the AMOC intensity and the northward extent of AAIW arises in part from ε_{Nd} reconstructions at intermediate depths from the tropical Atlantic, which show two opposite evolution behaviors: from the Last Glacial Maximum (LGM, 22 kyr Before Present, B.P.) to the Heinrich Stadial 1 (HS1, 17.5-14.7 kyr B.P.), ε_{Nd} decreases (becomes less radiogenic) in some cores [*Xie et al.*, 2012; *Huang et al.*, 2014], but increases (becomes more radiogenic) in some others [*Pahnke et al.*, 2008]. Understanding these opposite responses is critical for understanding the response of AAIW to deglacial AMOC variability.

To better understand the evolution of AAIW and the opposite ε_{Nd} changes in different tropical Atlantic records, we performed a transient ocean simulation for the last deglaciation (iPOP2-TRACE) [*Zhang*, 2016] under realistic climate forcings using a Nd-enabled ocean model. We find that the AAIW northward penetration in the tropical Atlantic is dominated by

AMOC strength but interpreting ε_{Nd} reconstructions is not as simple as suggested in previous studies because both the AAIW core depth and the influence of radiogenic bottom water from the Gulf of Mexico and the Caribbean Sea respond to variations in AMOC strength, influencing ε_{Nd} values in the tropical Atlantic. We describe the Nd implementation and experiments in section 2. We examine the deglacial AAIW evolution in our simulation and the associated physical mechanism in section 3. Section 4 discusses how the inconsistency in ε_{Nd} reconstructions can be understood in terms of the different depth and influence of the radiogenic water from the Gulf of Mexico and the Caribbean Sea. Finally, we summarize our findings in section 5.

2 Methods

2.1 Nd implementation

The Nd module is implemented in the ocean model (POP2) of Community Earth System Model (CESM) [*Hurrell et al.*, 2013] following *Rempfer et al.*, [2011]. Nd has three sources: riverine input, dust deposition and boundary source from continental margins. Dust and river sources enter the ocean at the surface ocean while the boundary source enters through the continental margins above 3,000m. Dust flux is prescribed using a model composite from *Mahowald et al.*, [2005]. We use global mean Nd concentration of 20 ug/g in the dust [*Goldstein et al.*, 1984; *Grousset et al.*, 1988, 1998] and 2% of which is released into the ocean [*Greaves et al.*, 1994]. River discharge is taken from the coupler of the model instead of being prescribed as in *Rempfer et al.*, [2011]. Nd concentration in river discharge is prescribed following *Goldstein and Jacobsen*, [1987] and 70% of the dissolved Nd in rivers is removed in estuaries [*Goldstein and Jacobsen*, 1987]. Nd flux from the continental margins is assumed to be a globally uniform value and we use 5.5×10^9 g/yr for the global total Nd source from the continental margins [*Rempfer et al.*, 2011]. ^{143}Nd and ^{144}Nd are simulated separately as two passive tracers and the fluxes for individual ^{143}Nd and ^{144}Nd are obtained by using prescribed isotopic ratio (IR = ^{143}Nd/^{144}Nd): IR_{dust} is prescribed following *Tachikawa et al.*, [2003] and IR_{river} and $IR_{boundary}$ are prescribed following *Jeandel et al.*, [2007].

The sink of Nd in the ocean is the reversible scavenging process. It describes the adsorption of Nd onto particles (particulate organic carbon (POC), opal, calcium carbonate ($CaCO_3$) and dust), settling downward along with these particles and the desorption from particles due to particle dissolution. In the bottom layer in the water column, if particles still exist, the Nd associated to these particles will be removed from the ocean. The balance between the dissolved Nd ($[Nd]_d$) and the particle related Nd ($[Nd]_p$) is described by equilibrium scavenging coefficient which is also prescribed following *Rempfer et al.*, [2011]. Therefore, the conservation equation for ^{143}Nd and ^{144}Nd is as follows:

$$\frac{\partial [Nd]_t^j}{\partial t} = S_{tot} - \frac{\partial\left(v\cdot[Nd]_p^j\right)}{\partial z} + T\left(\left[Nd\right]_t^j\right)(j = 143, 144)$$

The three terms on the right-hand side represent the total sources, the reversible scavenging, and the ocean transport, respectively. The settling velocity of particles, v, is chosen as 1000 m/yr as in *Rempfer et al.*, [2011]. Detailed description and parameterization are given in *Rempfer et al.*, [2011]. Our Nd module is not coupled with a marine biogeochemical model. We use export production of POC, opal and $CaCO_3$ from the biogeochemical component from Bern3D model and prescribe the remineralization profile following Rempfer et al. [2011]. Overall, our Nd concentration and ε_{Nd} capture the major features in the observations (in Section 2.2).

2.2 Nd module validation

Our Nd-enabled CESM can simulate the global distribution of both Nd concentration and ε_{Nd} reasonably well under present day climate forcing. We first run a present day control experiment (CTRL) forced by 1948-2007 atmospheric data from Coordinated Ocean-ice Reference Experiments [*Large and Yeager*, 2008]. Nd concentrations (both ^{143}Nd and ^{144}Nd) were initialized from zero. CTRL has been integrated for more than 4,000 model years until the Nd inventory has reached equilibrium. The Nd global inventory in CTRL is 3.64×10^{12}g, which is comparable to the observational estimates of 4.2×10^{12}g [*Tachikawa et al.*, 2003]. The mean residence time is 508 years, which is in the range reported previously [*Tachikawa et al.*, 2003]. Both simulated Nd concentration and ε_{Nd} in CTRL are also in reasonable agreement with a compilation of available observations [*van de Flierdt et al.*, 2016] (Figs.1, Fig.2 and Fig. S1) as discussed below.

Our model can simulate 64% of the Nd concentration observational points within ± 10 pmol/kg (70% in *Rempfer et al.*, [2011]) and 83% of the ε_{Nd} observational points with ± 3 ε_{Nd} unit (83% in Rempfer et al., [2011]). Nd concentration in CTRL captures the general feature of increasing with depth and also increasing along with the circulation pathway, consistent with observations (Fig. 1B and Fig. S1). Similar to observations [*Goldstein and Hemming*, 2003], ε_{Nd} values exhibits an inter-basin gradient as the North Pacific has the most radiogenic ε_{Nd} values, the North Atlantic has the least radiogenic values and the Indian and Southern Oceans have intermediate values (Fig. 1C and Fig.2). The linear regression coefficient between model ε_{Nd} and observational ε_{Nd} is 0.67 ($r^2 = 0.7$, N = 1699).

Since our study focuses on the Atlantic basin, especially the tropical Atlantic, we show several ε_{Nd} vertical profiles in the Atlantic (Fig.2). Overall, our model can simulate the vertical structure of ε_{Nd}, indicating the influences of water mass from different origins. For example, the zig-zag pattern in observations [*Goldstein and Hemming*, 2003] are successfully simulated in our model (Fig.2 profile 9 and 10), as AAIW and Antarctic Bottom Water (AABW) carry radiogenic ε_{Nd} northward and NADW carries unradiogenic ε_{Nd} southward. In particular, our model successfully captures the relative magnitude among different water masses, suggesting it can be used to study the relative changes of different water masses during the deglaciation. Another important feature is that our model is able to simulate the very radiogenic water from the Caribbean Sea (Fig. 2 profile 7) [*Osborne et al.*, 2014]. This turns out to be an important water mass that is the source of some of the discrepancies in the ε_{Nd} reconstructions, as will be discussed later in Section 4.

In spite of the overall agreement of the model simulation and the observations, there are also some deficiencies in the model. The Nd concentration at shallow depth is lower in the model than in observations and the vertical gradient is larger in the model than the observations (Fig.1B and D, Fig.S1), as in the case of *Rempfer et al.*, [2011]. These deficiencies in simulating surface Nd is due partly to our choice of model parameters that optimize ε_{Nd} instead of Nd, as in Rempfer et al., [2011]. With extensive sensitivity experiments, Rempfer et al., [2011] shows that it is impossible to optimize the simulation for both Nd concentration and ε_{Nd} simultaneously. They chose the parameters that yield the best ε_{Nd} simulation, since ε_{Nd} is the proxy used for reconstructing past circulations. These parameter values are also used in our model setting. Overall, our model can simulate the major ε_{Nd} features of the main water masses over both global scale and local scale of the tropical Atlantic and therefore should help us interpret ε_{Nd} reconstructions in the tropical Atlantic in the past.

2.3 Transient deglacial simulation

The transient simulation (iPOP2-TRACE) is carried out using Nd-enabled ocean-alone model CESM-POP2 to simulate the global ocean evolution from the LGM (21ka) to the late Bølling-Allerød Interstadial (13ka) under realistic surface forcings. The model was first spun up under LGM condition and then integrated to the present under surface climate forcing taken from a transient simulation in a fully coupled climate model (TRACE21k, using CCSM3), which reproduced many features in last deglaciation [*Liu et al.*, 2009; *He*, 2011]. The horizontal resolution is nominally 3° and it has 60 vertical layers with a 10-m resolution in the upper 200m, increasing to 250m below 3000m. Detailed experiment descriptions are described in *Zhang*, [2016].

We keep Nd sources and ε_{Nd} in Nd sources unchanged during the deglacial simulation iPOP2-TRACE. Surface dust flux and origin [*Grousset et al.*, 1998; *Wolff et al.*, 2006; *Lupker et al.*, 2010] and river runoff magnitude and origin [*Harris and Mix*, 1999; *Burton and Vance*, 2000; *Nurnberg and Tiedemann*, 2004; *Lézine et al.*, 2005; *Stoll et al.*, 2007; *Rincon-Martinez et al.*, 2010] were reported to be changing throughout time. Boundary source of Nd is not well constrained [*Amakawa et al.*, 2000; *Johannesson and Burdige*, 2007; *Rickli et al.*, 2010], therefore it is hard to estimate the change in the past, although it is highly likely to happen due to changes in different processes such as groundwater discharge [*Zektser and Loaiciga*, 1993; *Johannesson and Burdige*, 2007] and continental erosion [*Tütken et al.*, 2002]. Results from a modeling study suggest that changes in the sources are unlikely to be important, as the magnitude of the reconstructed glacial-deglacial ε_{Nd} variations is hard to obtain by only changing the Nd sources and/or ε_{Nd} in Nd sources [*Rempfer et al.*, 2012b]. We also keep the particle fields as the present, with no change throughout the simulation. This choice, although is not very realistic [*Kohfeld et al.*, 2005], is limited by our model capability which is not fully coupled with a marine ecosystem model. This limitation will be addressed in a future study when an active marine ecosystem model is enabled. Here, our simplified model has the advantage that the change of the ocean circulation is the only factor that affects ε_{Nd} distribution, enabling us to focus on the influence of ocean circulation.

3 Coherent AAIW response and AMOC strength

3.1 Reduced AAIW northward penetration but increased depth and thickness of AAIW water mass during weaker AMOC

In the modern ocean, AAIW can be identified by a low salinity (or radiogenic ε_{Nd}) tongue originating from the subantarctic surface ocean extending northward at the intermediate depth [*Talley*, 1996] (Fig. 3). Here, consistent with convention, we define σ_{AAIW} as the potential density at the salinity minimum point in the South Atlantic mean potential temperature-salinity (θ-S) diagrams. For convenience, the AAIW depth is defined as the zonal mean depth of σ_{AAIW} at the equatorial Atlantic. The AAIW ε_{Nd} is defined as the zonal mean ε_{Nd} value at σ_{AAIW} (or AAIW depth) at the equatorial Atlantic. The σ_{AAIW} in CTRL is 27.36 kg/m^3, which is comparable to the observation value of 27.3 kg/m^3 [*Talley*, 1996]. The isopycnal line of σ_{AAIW} is also consistent with the low salinity and the high ε_{Nd} tongue in the Atlantic (Fig. 3, green line), suggesting that this is a good approximation for the location of AAIW core layer. The AAIW depth in CTRL is 778 meters, which is also in the range of modern observations [*Talley*, 1996].

iPOP2-TRACE simulates the key oceanic changes during the last deglaciation. The simulated AMOC collapses during HS1 in response to freshwater forcing in the North Atlantic and then recovers rapidly in the Bølling-Allerød warming (BA, ~14.5 kyr B.P.) (Fig. 4B, black), consistent with $^{231}Pa/^{230}Th$ records from Bermuda Rise [*McManus et al.*, 2004](Fig. 4B, green) and the original coupled model simulation [*Liu et al.*, 2009].

In iPOP2-TRACE, the northward penetration of AAIW in the Atlantic is closely linked to the change of AMOC. During LGM and HS1, σ_{AAIW} surface also tends to follow the low salinity, or the radiogenic ε_{Nd}, tongue of AAIW (green lines in Figs. 5C and D), as in CTRL. To better quantify the northward penetration of AAIW in the Atlantic, we estimate the AAIW northward penetration latitude using Atlantic zonal mean ε_{Nd}: we first calculate the maximum ε_{Nd} value in the South Atlantic above 1,200 meters, then we find the latitude that ε_{Nd} value of 1.3 ε_{Nd} unit less than the maximum can reach above 1,200 meters. The AAIW northward extent varies over an approximately 15^{o} latitude range during the deglaciation (Fig. 4C blue dots), with a high positive correlation with the AMOC intensity (Fig. 4B black). AAIW in the Atlantic reaches 2°N during the LGM, and withdraws southward after 19ka, when the AMOC starts to decrease in response to the meltwater input in the North Atlantic. By late HS1, the AAIW retreats to its southernmost latitude of 17°S, followed by a rapid intrusion during the BA to 1°N, in response to the AMOC recovery. This HS1 southward retreat of the AAIW tongue is also obvious in the Atlantic zonal mean salinity or ε_{Nd} (Fig. 5 C and D) and the horizontal distribution of ε_{Nd} at σ_{AAIW} surface (Fig. 5E and F).

Physically, the change of latitudinal extent is also consistent with that of the cross-equator transport of the AAIW (Fig. 4B red), which is defined as the northward transport between the isopycnal surfaces of $\sigma_{AAIW}\pm0.5$, and more generally, the subsurface component of the NBC, in the model. The AAIW transport is reduced during the HS1 and increased again during the BA, also following the AMOC [*Nace et al.*, 2014]. This result is insensitive to the choice of density interval (d), between σ_{AAIW} – d and σ_{AAIW} + d, because similar results are produced with density intervals (d) ranging from 0.1 to 0.4 (Fig. S2).

The equatorial Atlantic ε_{Nd} at the AAIW depth (AAIW ε_{Nd}) also varies closely with the AAIW northward penetration, as hypothesized in previous ε_{Nd} reconstructions [*Pahnke et al.*, 2008; *Xie et al.*, 2012; *Huang et al.*, 2014]. Our model shows an almost linear relationship between the equatorial AAIW ε_{Nd} (Fig. 4D solid black, which follows σ_{AAIW} and varies with depth) and the northward penetration latitude of AAIW (Fig. 4C navy dot), with decreased ε_{Nd} during HS1 and its subsequent increase during BA corresponding to the southward withdraw and the subsequent northward re-advance in the penetration latitude, respectively. In the model, we calculate the ε_{Nd} of the AAIW southern end-member, which is the average ε_{Nd} in the AAIW production region. It remains unchanged at -8.3 during the deglaciation prior to BA and shifts abruptly to -9.1 during BA due to the quick AMOC recovery during BA, which brings unradiogenic ε_{Nd} water from the North Atlantic to the Southern Ocean. The evolution of the ε_{Nd} difference between the equatorial Atlantic and its southern end-member (Fig. 4D, red) is similar to the evolution of the ε_{Nd} in the equatorial Atlantic (Fig. 4D, solid black). Therefore, ε_{Nd} in the equatorial Atlantic at AAIW depth can indeed be used as an indicator for AAIW northward penetration in the Atlantic.

Another important feature of AAIW is that its depth changes significantly during the last deglaciation in iPOP2-TRACE. The AAIW depth is also closely linked to the AMOC evolution, deepening from around 230-m during LGM to around 670-m during HS1, shoaling back to 240-m during BA (Fig.4C red) and deepening again slowly to ~530-m in the Holocene (Fig. 4C triangle on right Y axis), which is consistent with the present day observation [*Talley*, 1996]. This deepening of AAIW from LGM to HS1 has been illustrated in previous modeling studies [e.g. *Vallis*, 2000; *Wolfe and Cessi*, 2010]. When the surface density in the source region of NADW is between the surface density in the source region of AAIW and AABW ($\sigma_{AAIW} < \sigma_{NADW} < \sigma_{AABW}$), which is the case during LGM in our simulation (Fig. 4A), NADW fills the mid-depth and AAIW is shallow and partially entrained in the main thermocline. However, when the surface density in the source region of NADW is less than AAIW, which is the case during HS1 in our simulation, as no NADW is produced due to the melt water input to the North Atlantic (Fig. 4A), AAIW fills the middepth between abyssal and main thermocline. Therefore, AAIW becomes deeper and thicker during HS1. In addition, this magnitude of deepening of middepth water during HS1 has also been suggested by the deglacial attmospheric radiocarbon decline [*Hain et al.*, 2014]. Finally, the Holocene deepening compared with the glacial period may be caused partly by the sea ice retreat in the Southern Ocean [*Ferrari et al.*, 2014].

The depth change of AAIW core layer may also contribute to ε_{Nd} change at a fixed depth. As the AAIW deepens, any site above (below) AAIW core layer would experience a less (more) radiogenic ε_{Nd} shift, which may complicate the interpretation of ε_{Nd} evolution as AAIW northward penetration. However, the ε_{Nd} in the western boundary of equatorial Atlantic shows a change of about 1 unit ε_{Nd} change from the LGM to the HS1 at a fixed intermediate depth of 1000m (Fig. 4D black dash) (similar at 500m and 800m, not shown), and this change at fixed depth is comparable with the ε_{Nd} change at the AAIW core depth that changes with time (Fig.4D black solid). Therefore, the ε_{Nd} change from the tropical Atlantic is dominated by the change in the AAIW northward penetration change rather than AAIW depth change.

Overall, our model shows a coherent response between the AMOC intensity and the AAIW northward penetration latitude, northward transport, AAIW ε_{Nd} value and AAIW depth in iPOP2-TRACE. These relationships are robust in the model and have been reproduced in several idealized hosing experiments (Fig. S4 and S5). Our simulation is also consistent with a climate model of intermediate complexity [*Rempfer et al.*, 2012a] (their Figure 12a), where the zonal-mean ε_{Nd} becomes more radiogenic with a maximum increases of 4 ε_{Nd} units in the upper 1,200 meters of the equatorial Atlantic and decreases at greater depths for a transitions from an NADW-on state to an NADW-off state.

3.2 Mechanism

How does a weaker AMOC reduce the AAIW northward penetration in the Atlantic? Intuitively, one might think the AAIW northward penetration of AAIW is determined mainly by its production rate: a larger AAIW production rate would favor a stronger northward penetration towards the North Atlantic. This is not the case in iPOP2-TRACE: AAIW northward penetration is not controlled by upstream AAIW production. We compare the AAIW subduction rate, which is the subduction across the base of the ocean mixed layer in the South Atlantic AAIW formation region [*Goes et al.*, 2008]. The AAIW subduction rate is 4.6 Sv during LGM and 6.0 Sv during HS1 in iPOP2-TRACE, indicating the upstream AAIW production during HS1 is not lower but even higher. This stronger HS1 AAIW production rate during HS1 also occurs in the fully coupled experiment TRACE21k, which shows a subduction rate of 16 Sv during LGM (consistent with *Wainer et al.*, [2012]) and 19 Sv during HS1, although the overall magnitudes of the subduction rate are different. The relatively smaller magnitude of AAIW subduction in the ocean-alone simulation (iPOP2-TRACE) than in the fully coupled simulation (TRACE21k) is because the AAIW subduction rate depends on the mixed layer depth, which is much smaller in iPOP2-TRACE than in TRACE21k, probably because that iPOP2-TRACE is forced by monthly atmospheric forcings, in which the high frequency signals are filtered out. Regardless of these differences, the results from both simulations indicate that the retreat of AAIW northward penetration during HS1 cannot be caused by AAIW formation in the Southern Ocean.

Since the meltwater flux to the North Atlantic can reverse the density contrast between AAIW and NADW such that AAIW becomes heavier than NADW, it could encourage the northward penetration of AAIW and the southward compensating flow from the North Atlantic above AAIW, forming a reversed counterclockwise shallow overturning cell that circulates in the opposite direction to the modern AMOC [*Keeling and Stephens*, 2001; *Saenko et al.*, 2003; *Weaver et al.*, 2003]. In our model, the higher surface density in the NADW formation region during LGM (σ_{NADW}=28.5 kg/m^3 > σ_{AAIW} =28.2 kg/m^3) is indeed reduced to lower than that of AAIW during HS1 (σ_{AAIW}=28.0 kg/m^3 > σ_{NADW}=26.8 kg/m^3) (Fig. 4A). However, no reversed AAIW cell is generated (Fig. 5B). The detailed mechanism of the reversed AAIW cell remains to be fully understood in future studies. Here, we note that, during LGM, the AAIW lies above NADW, contributing to the return flow of NADW as in modern observation [*Lumpkin and Speer*, 2003]; in response to the freshwater input during HS1, the southward export of NADW at depth collapses, which then reduces the compensating flow in the upper ocean, including AAIW. As such, the AAIW retreats to south of the equator during HS1 (Fig. 5 B, D and F). This response is consistent with the present day observational [*Zhang et al.*, 2011] and modeling studies of the multi-decadal variability of the NBC, which is found to be determined predominantly by the changes of the AMOC and NADW formation [*Rühs and Getzlaff*, 2015].

Our study suggests a remote dynamical control on the AAIW northward penetration from the North Atlantic, as opposed to a local control of AAIW production and transport from the Southern Ocean. Typically, the AAIW is transported northward first through the southern subtropical gyre circulation and then across the equator by the western boundary current, as in modern observations [*Schmid et al.*, 2000]. During the LGM, the AAIW flows northwestward to ~20^{o}S in a broad interior pathway, following the counterclockwise subtropical gyre in the South Atlantic at intermediate depth (Fig. 6A); most of the AAIW water, however, recirculates back through the southward Brazil Current along the western boundary (Fig. 6B). A small residual of AAIW advances beyond 20^{o}S northward along the western boundary into the tropical Atlantic; this part of AAIW then crosses the equator as a part of the subsurface component of the NBC along the western boundary, generating a low salinity/high ε_{Nd} tongue there. The AAIW penetrates across the equator only in the western boundary current because the cross-equator penetration is largely prohibited in the interior ocean due to the conservation of potential vorticity [*McCreary and Lu*, 2001]. During HS1, there is little AAIW transported across the equator (Fig. 6D), confining the low salinity/high ε_{Nd} tongue south of the equator (Fig. 5D). Upstream in the subantarctic South Atlantic, however, the northward transport of AAIW is actually increased relative to the LGM (Figs. 6B and 6D); this increased AAIW transport, however, is returned southward almost entirely in the Brazil Current, leaving little AAIW penetrating into the equatorial Atlantic (Fig.6D). Thus, the deglacial evolution of the AAIW penetration to the tropical Atlantic appears to be determined predominantly by the remote processes in the North Atlantic, rather than by the local forcing in the South Atlantic subantarctic region. This remote control of AAIW in the Atlantic is similar to that in the Pacific, where the cross-equator penetration of AAIW is caused predominantly by the opening of the Indonesia Throughflow, rather than the climate forcing in the South Pacific subantarctic region [*McCreary and Lu*, 2001]. We also did an idealized hosing experiment (not shown), in which constant fresh water forcing of 1Sv is added to North Atlantic for the first 100 years and then removed. It shows similar equatorial ε_{Nd} response as in iPOP2-TRACE and ε_{Nd} lags AMOC change for 30-40 years.

4 Reconciling ε_{Nd} reconstructions controversy with core depth

As noted above, available tropical ε_{Nd} reconstructions show contradictory ε_{Nd} evolutions across the last deglaciation. The ε_{Nd} reconstruction from the Tobago Basin (MD99-2198, 12.09°N, 61.23°W, 1330m) [*Pahnke et al.*, 2008] shows an increase (becomes more radiogenic) during the HS1 (Fig. 4F), which was interpreted as enhanced northward advection of AAIW. However, ε_{Nd} records from the Florida Strait (KNR166-2-26JPC, 24°19.62'N, 83°15.14'W, 546m) [*Xie et al.*, 2012] (Fig. S3C) and the Demerara Rise (KNR197-3-46CDH, 7.836°N, 53.663°W, 947m) [*Huang et al.*, 2014] (Fig. 4E) show decreases (become less radiogenic) during the HS1, and were interpreted to indicate decreased penetration of AAIW into tropical North Atlantic. The controversy may be due to deficiencies of each data site. On the one hand, it was argued that MD99-2198 lies beneath the modern AAIW depth range and fails to record the AAIW northward penetration signals [*Xie et al.*, 2012]. On the other hand, present day hydrographic data from the Gulf of Mexico shows much warmer and saltier water mass than AAIW, suggesting that if any AAIW has arrived at this site, it has already been modified by other water masses. Therefore, site KNR166-2-26JPC from the Florida Strait has been suggested not ideally situated to record the deglacial AAIW changes [*Pena et al.*, 2013; *Osborne et al.*, 2014].

Our model reproduces the ε_{Nd} evolutions at different sites from intermediate depth. The ε_{Nd} from the Demerara Rise (~950m) (Fig. 4E and S3 A, B) and from the Florida Strait (~540m)

(Fig.S3 C) exhibit less radiogenic excursion during HS1, while ε_{Nd} from the Tobago Basin (~1330m) shows a more radiogenic shift during HS1 (Fig. 4F). Our model is able to simulate the diverse ε_{Nd} evolutions consistent with the reconstructions at these three tropical North Atlantic sites and suggest that the opposite ε_{Nd} evolutions at these locations are physically consistent with a common deglacial ocean circulation change. The interpretation, however, is more complex than suggested in previous studies because it involves both the change of the AAIW depth and the radiogenic water from the Gulf of Mexico and the Caribbean Sea, as discussed below.

Our model simulation shows that the less radiogenic shift of ε_{Nd} from the Florida Strait site (KNR166-2-26JPC) during HS1 [*Xie et al.*, 2012] is due to the reduced influence of the radiogenic water from the bottom in the Gulf of Mexico and the Caribbean Sea. Deep water from the Gulf of Mexico and the Caribbean Sea features very radiogenic ε_{Nd} sources from boundary exchange as discussed in Section 2.2 [*Jeandel et al.*, 2007; *Osborne et al.*, 2014]. During LGM, active AMOC drives strong upwelling in this region (Fig. 7A black contour), which, in turn, influences the shallow layers with very radiogenic ε_{Nd} water in this region and the nearby open ocean in the subtropical North Atlantic. The influence of this regional radiogenic ε_{Nd} source can also be seen in the Atlantic zonal mean ε_{Nd} as a high ε_{Nd} center located at 600m-900m from 20°N to 40°N (Fig. 5C) (also in Fig. 3 in modern CTRL). During HS1, however, this radiogenic ε_{Nd} bottom water is trapped in the bottom locally because of reduced upwelling (Fig. 7A black contour). This leads to a great reduction in the transport of radiogenic ε_{Nd} water from bottom to shallow layers and therefore, a unradiogenic ε_{Nd} shift in the upper 1,500 m in the Gulf of Mexico and the Caribbean Sea (Fig. 7 A color contour) and, eventually, in the upper 1,000 m in subtropical North Atlantic as there is no more a radiogenic ε_{Nd} center in subtropical North Atlantic in the zonal mean ε_{Nd} (Fig. 5D). Furthermore, the ε_{Nd} from the Florida Strait site is dominated by radiogenic horizontal advection (Fig. S7 A) by an eastward flow from the Gulf of Mexico (Fig. S7 B). ε_{Nd} at this site experiences an unradiogenic shift during HS1 because with reduced input of deep radiogenic waters, the upper ocean in the Gulf of Mexico becomes less radiogenic and at the same time, the eastward flow also becomes weaker (Fig. S7 B). Thus, ε_{Nd} variations in the Florida Strait are not due to variations in AAIW as previously suggested [*Xie et al.*, 2012]. Overall, the relationship between the weakened AMOC and the weakened influence from the regional radiogenic ε_{Nd} influence from the Gulf of Mexico and the Caribbean Sea is also robust in our idealized hosing experiment (Fig. S5 C and D), although detailed dynamics that relates the weakened AMOC and the reduced upwelling in the Gulf of Mexico and Caribbean Sea remains to be further studied.

Our model simulation further suggests that the opposite ε_{Nd} behaviors at two nearby sites from the Demerara Rise and the Tobago Basin discussed above are caused by the different depths of the sediment cores as well as the influence of radiogenic ε_{Nd} water from the Caribbean Sea. Both locations experience similar ε_{Nd} change in the upper 2,000m (Fig. 7 C and D). During the LGM, the Demerara Rise site is located in the lower limb of AMOC (as shown in southward meridional velocity in Fig. 8A and 9C), with water transported from the subtropical North Atlantic and the Caribbean Sea. Starting from 19ka, AMOC begins to decrease in response to the fresh water forcing applied to the North Atlantic, ε_{Nd} in the subtropical North Atlantic becomes less radiogenic due to the reduced influence of the radiogenic source water from the bottom of the Gulf of Mexico and the Caribbean Sea as discussed above. In the meantime, the meridional velocity also begins to decrease (Fig. 9C), leading to a decrease in the radiogenic ε_{Nd} advection term (Fig. 9A). During HS1, the flow is almost stagnant (Fig. 9C) and all the ε_{Nd} tendency terms are greatly reduced compared with LGM (Fig. 9A). Therefore, the less radiogenic shift in ε_{Nd}

during HS1 from the Demerara Rise is due to the reduced influence of radiogenic water from bottom of the Gulf of Mexico and the Caribbean Sea as well as the reduced southward flow, instead of the retreat of northward advection of AAIW suggested in *Huang et al.*, [2014].

The Tobago Basin site is about 400 meters deeper than the Demerara Rise site and is mainly influenced by the NADW from the north, which features unradiogenic ε_{Nd} values. Although NADW ε_{Nd} is complicated by distinct west and east NADW source waters [van de Flierdt et al., 2016], in our simulation, changes in the relative contribution from west versus east NADW formation does not have much influence on the NADW ε_{Nd} value (SI. text 2), which is consistent with the finding that the influence of the endmember ε_{Nd} change is rather small compared with ε_{Nd} changes due to changes in watermass distribution [*Rempfer et al.*, 2012a]. During LGM, strong southward western boundary current contributes to the unradiogenic ε_{Nd} advections at the Tobago Basin site (Fig. 8B and Fig. 9B). When AMOC collapsed during HS1, this unradiogenic ε_{Nd} advection of NADW is also reduced (Fig. 9B and D), which then contributes to the more radiogenic shift of ε_{Nd} during HS1 as in the ε_{Nd} reconstruction. In addition, circulation change in the Caribbean Sea also contributes to the more radiogenic ε_{Nd} shift in the Tobago Basin during HS1. During LGM, flow at the location where the Caribbean Sea connects with the Atlantic (12°N, 75°W, 1330m) is westward and therefore leads to a less radiogenic ε_{Nd} advection into the the Caribbean Sea (Fig. 8B and Fig. S6A). During HS1, however, the westward flow is changed to eastward flow out of the Caribbean Sea, because of the reduced deep west boundary current (Fig. 8D and Fig. S6B). This eastward flow out of the Caribbean Sea transports radiogenic ε_{Nd} water from the Caribbean Sea out to influences the Tobago Basin site. Therefore, the more radiogenic ε_{Nd} shift during HS1 in Tobago Basin site is caused by both the retreat of the unradiogenic ε_{Nd} NADW and the leak of radiogenic ε_{Nd} water from the Caribbean Sea. Again, variations in the northward extent of AAIW did not control the ε_{Nd} evolution in this Tobago Basin site, contrary to what was suggested previously [*Pahnke et al.*, 2008].

The discussion above suggests that deglacial ε_{Nd} in the low latitude North Atlantic at the depth of modern AAIW can be complicated by the radiogenic ε_{Nd} end-member form the Gulf of Mexico and the Caribbean Sea. From LGM to HS1, our model ε_{Nd} exhibits an unradiogenic shift above around 1,100-m and a more radiogenic shift from 1,100-m to 2,000-m at both the Demerara Rise and the Tobago Basin (Fig.7 C and D), consistent with the respective proxy records. Above 1,100-m, low latitude North Atlantic ε_{Nd} can be influenced by both southern sourced water of AAIW in the upper layers and northern sourced water from the Caribbean Sea, both of which become weaker and lead to an unradiogenic shift of ε_{Nd} when AMOC strength is reduced. Below 1,100-m, water is influenced mainly by the NADW as well as water from the Caribbean Sea. The retreat of NADW and the advance of the Caribbean Sea water both lead to a radiogenic shift of ε_{Nd} during reduced AMOC. Therefore, radiogenic ε_{Nd} water from the Gulf of Mexico and the Caribbean Sea provides effectively the third ε_{Nd} end-member in addition to the radiogenic ε_{Nd} south sourced AAIW and unradiogenic ε_{Nd} north sourced water. This third source should be taken into consideration when interpreting ε_{Nd} reconstructions from low latitude North Atlantic at modern intermediate depth.

It should also be pointed out that the interpretation of the deglacial ε_{Nd} records from the tropical Atlantic can also be complicated by the changing depth of the AAIW during the deglaciation. Our model shows a much shallower AAIW during LGM than the present day (Fig. 4C). Sites located at modern AAIW depth may not be influenced by AAIW in the past. In iPOP2-TRACE, in the western boundary of equatorial Atlantic, for the upper 900 meters, flow is northward which contributes to a radiogenic ε_{Nd} advection, indicating an AAIW influence. Therefore, we suggest that ε_{Nd} reconstructions shallower than 900 meters from equatorial and tropical Atlantic are more suitable to reconstruct past AAIW northward penetration change. The complicated mechanisms controlling ε_{Nd} reconstruction at different sites from the tropical North Atlantic, however, also indicates that more reconstructions from different locations and depths are needed to infer past circulation changes as suggested by *van de Flierdt et al.*, [2016].

5 Conclusions

Overall, our transient Nd-enabled ocean model simulation suggests a coherent AAIW response to the change of AMOC strength. The northward AAIW penetration in the tropical Atlantic is determined predominantly by the AMOC intensity or climate in the high latitude of the North Atlantic remotely, with a stronger AMOC enhancing AAIW northward penetration (Fig. 10 A and B). In addition, AAIW water mass sinks to a greater depth and dominates a wider water depth range in response to the freshening of NADW. Our results suggest that AAIW is a critical part of the return flow of the southward flowing NADW and, in turn, the global thermohaline circulation, and therefore can contribute significantly to the global climate change. Also, monitoring changes of AAIW can contribute to our understanding of climate changes in the past and help future projections.

During HS1, the reduced AMOC strength is caused by fresh water forcing in the North Atlantic. Under this North Atlantic buoyancy forcing scenario, we find that AAIW becomes deeper when AMOC is weaker. *Toggweiler and Samuels*, [1995] suggests that NADW formation in the North Atlantic is also controlled by wind forcing in the Southern Ocean: weaker winds over Drake Passage will lead to weaker NADW formation. Interestingly, the pycnocline depth becomes shallower under weaker Southern Ocean wind forcing. This relationship between pycnocline and AMOC strength under Southern Ocean wind forcing is opposite to our finding under North Atlantic buoyancy forcing. Therefore, the response of the circulation at middepth to the forcings from the North Atlantic and the Southern Ocean needs to be further studied.

In addition, ε_{Nd} reconstructions from the tropical and subtropical North Atlantic from within and near modern AAIW depths do not inform us about northward AAIW extent as previously assumed. Our simulation reproduces the contrasting deglacial ε_{Nd} evolutions at three intermediate-depth sites in the tropical North Atlantic. The inconsistency among reconstructions relates to the individual site locations and depths. With the AAIW depth changing in the past, core sites bathed by AAIW in present day, such as the Demerara Rise site, may not be influenced by AAIW in the past. In addition, our results point out the importance the radiogenic ε_{Nd} water from the Gulf of Mexico and the Caribbean Sea as the third end-member for regulating ε_{Nd} values at intermediate depth in tropical North Atlantic, which complicates the interpretation of ε_{Nd} reconstruction in the tropical North Atlantic. During the AMOC-on state (LGM), upwelling in the Gulf of Mexico and the Caribbean Sea brings very radiogenic water from the bottom to shallow depth, influencing the upper 1,000 m of the tropical and subtropical Atlantic (Fig. 10 C). During the AMOC-off state (HS1), this upwelling is greatly reduced and the upper 1,000 m subtropical and tropical Atlantic ε_{Nd} experience an unradiogenic shift (Fig. 10 D), which, combined with a weak deep western boundary current, lead to the unradiogenic shift in reconstruction of the Demerara Rise site (Fig. 10C and D). The radiogenic shift in the reconstruction of the Tobago Basin site during HS1 is due to the reduced deep western boundary current as well as leakage of radiogenic water from the Caribbean Sea (Fig. 10E and F).

Therefore, we cannot interpret ε_{Nd} reconstructions from the tropical Atlantic within and near modern AAIW depth without taking the influence of radiogenic water from the Gulf of Mexico and the Caribbean Sea into consideration. Eventually, more reconstructions from different depths and latitudes, and comparison of these records to simulations using Nd-enabled models, will help to improve our understanding of past circulation.

Acknowledgements: We are especially grateful to two reviewers and the editor for their constructive comments. We thank B. Otto-Bliesner and E. Brady for their support of the work, and we thank Dr J. Zhu for helpful discussions. This study was supported by the US NSF P2C2 (NSF 1401778 and NSF1401802), DOE DE-SC0006744 and NSFC 41630527 and 41130105. F.J. acknowledges support by the Swiss National Science Foundation. D. O. acknowledges support from the WHOI Investing in Science Program and the US NSF. Computing resources (ark:/85065/d7wd3xhc) were provided by the Climate Simulation Laboratory at NCAR's Computational and Information Systems Laboratory (CISL), sponsored by the National Science Foundation and other agencies. Data used to produce the results in this study can be obtained from HPSS at CISL: /home/sgu28/iPOP_TRACE.

References

Amakawa, H., D. S. Alibo, and Y. Nozaki (2000), Nd isotopic composition and REE pattern in the surface waters of the eastern Indian Ocean and its adjacent seas, *Geochim. Cosmochim. Acta*, *64*(10), 1715–1727, doi:10.1016/S0016-7037(00)00333-1.

Burton, K. W., and D. Vance (2000), Glacial-interglacial variations in the neodymium isotope composition of seawater in the Bay of Bengal recorded by planktonic foraminifera, *Earth Planet. Sci. Lett.*, *176*(3–4), 425–441, doi:10.1016/S0012-821X(00)00011-X.

Came, R. E., D. W. Oppo, W. B. Curry, and J. Lynch-Stieglitz (2008), Deglacial variability in the surface return flow of the Atlantic meridional overturning circulation, *Paleoceanography*, *23*(1), doi:10.1029/2007PA001450.

Ferrari, R., M. F. Jansen, J. F. Adkins, A. Burke, A. L. Stewart, and A. F. Thompson (2014), Antarctic sea ice control on ocean circulation in present and glacial climates., *Proc. Natl. Acad. Sci. U. S. A.*, *111*(24), 8753–8, doi:10.1073/pnas.1323922111.

van de Flierdt, T., L. F. Robinson, J. F. Adkins, S. R. Hemming, and S. L. Goldstein (2006), Temporal stability of the neodymium isotope signature of the Holocene to glacial North Atlantic, *Paleoceanography*, *21*(4), doi:10.1029/2006PA001294.

van de Flierdt, T., A. M. Griffiths, M. Lambelet, S. H. Little, T. Stichel, and D. J. Wilson (2016), Neodymium in the oceans: a global database, a regional comparison and implications for palaeoceanographic research, *Philos. Trans. R. Soc. A Math. Phys. Eng. Sci.*, *374*(2081), 20150293, doi:10.1098/rsta.2015.0293.

Foster, G. L., D. Vance, and J. Prytulak (2007), No change in the neodymium isotope composition of deep water exported from the North Atlantic on glacial-interglacial time scales, *Geology*, *35*(1), 37, doi:10.1130/G23204A.1.

Goes, M., I. Wainer, P. R. Gent, and F. O. Bryan (2008), Changes in subduction in the South Atlantic Ocean during the 21st century in the CCSM3, *Geophys. Res. Lett.*, *35*(6), L06701, doi:10.1029/2007GL032762.

Goldstein, S., and S. Hemming (2003), Long-lived isotopic tracers in oceanography, paleoceanography, and ice-sheet dynamics, *Treatise on geochemistry*, *6*(6), 453–489.

Goldstein, S. J., and S. B. Jacobsen (1987), The Nd and Sr isotopic systematics of river-water dissolved material: Implications for the sources of Nd and Sr in seawater, *Chem. Geol. Isot. Geosci. Sect.*, *66*(3–4), 245–272, doi:10.1016/0168-9622(87)90045-5.

Goldstein, S. L., R. K. O'Nions, and P. J. Hamilton (1984), A Sm-Nd isotopic study of atmospheric dusts and particulates from major river systems, *Earth Planet. Sci. Lett.*, *70*(2), 221–236, doi:10.1016/0012-821X(84)90007-4.

Greaves, M., P. Statham, and H. Elderfield (1994), Rare earth element mobilization from marine atmospheric dust into seawater, *Mar. Chem.*, *46*(3), 255–260.

Grousset, F. E., P. E. Biscaye, a. Zindler, J. Prospero, and R. Chester (1988), Neodymium isotopes as tracers in marine sediments and aerosols: North Atlantic, *Earth Planet. Sci. Lett.*, *87*(4), 367–378, doi:10.1016/0012-821X(88)90001-5.

Grousset, F. E., M. Parra, A. Bory, P. Martinez, P. Bertrand, G. Shimmield, and R. M. Ellam (1998), Saharan wind regimes traced by the Sr-Nd isotopic composition of subtropical Atlantic sediments: Last Glacial Maximum vs Today, *Quat. Sci. Rev.*, *17*(4–5), 395–409, doi:10.1016/S0277-3791(97)00048-6.

Gruber, N. et al. (2009), Oceanic sources, sinks, and transport of atmospheric CO2, *Global Biogeochem. Cycles*, *23*(1), doi:10.1029/2008GB003349.

Hain, M. P., D. M. Sigman, and G. H. Haug (2014), Distinct roles of the Southern Ocean and North Atlantic in the deglacial atmospheric radiocarbon decline, *Earth Planet. Sci. Lett.*, *394*, 198–208, doi:10.1016/j.epsl.2014.03.020.

Harris, S., and A. Mix (1999), Pleistocene Precipitation Balance in the Amazon Basin Recorded in Deep Sea Sediments, *Quat. Res.*, *26*(1999), 14–26, doi:10.1006/qres.1998.2008.

He, F. (2011), SIMULATING TRANSIENT CLIMATE EVOLUTION OF THE LAST DEGLACIATION WITH CCSM3.

Hendry, K. R., X. Gong, G. Knorr, J. Pike, and I. R. Hall (2016), Deglacial diatom production in the tropical North Atlantic driven by enhanced silicic acid supply, *Earth Planet. Sci. Lett.*, *438*, 122–129, doi:10.1016/j.epsl.2016.01.016.

Howe, J. N. W., A. M. Piotrowski, D. W. Oppo, K.-F. Huang, S. Mulitza, C. M. Chiessi, and J. Blusztajn (2016), Antarctic Intermediate Water circulation in the South Atlantic over the past 25,000 years, *Paleoceanography*, doi:10.1002/2016PA002975.

Huang, K.-F., D. W. Oppo, and W. B. Curry (2014), Decreased influence of Antarctic intermediate water in the tropical Atlantic during North Atlantic cold events, *Earth Planet. Sci. Lett.*, *389*, 200–208, doi:10.1016/j.epsl.2013.12.037.

Hurrell, J. W. et al. (2013), The community earth system model: A framework for collaborative research, *Bull. Am. Meteorol. Soc.*, *94*(9), 1339–1360, doi:10.1175/BAMS-D-12-00121.1.

Ito, T., M. Woloszyn, and M. Mazloff (2010), Anthropogenic carbon dioxide transport in the Southern Ocean driven by Ekman flow., *Nature*, *463*(7277), 80–83, doi:10.1038/nature08687.

Jacobsen, S. B., and G. J. Wasserburg (1980), Sm-Nd isotopic evolution of chondrites, *Earth Planet. Sci. Lett.*, *50*(1), 139–155, doi:10.1016/0012-821X(80)90125-9.

Jeandel, C., T. Arsouze, F. Lacan, P. Techine, and J. Dutay (2007), Isotopic Nd compositions and concentrations of the lithogenic inputs into the ocean: A compilation, with an emphasis on the margins, *Chem. Geol.*, *239*(1–2), 156–164, doi:10.1016/j.chemgeo.2006.11.013.

Johannesson, K. H., and D. J. Burdige (2007), Balancing the global oceanic neodymium budget: Evaluating the role of groundwater, *Earth Planet. Sci. Lett.*, *253*(1–2), 129–142, doi:10.1016/j.epsl.2006.10.021.

Keeling, R., and B. Stephens (2001), Antarctic sea ice and the control of Pleistocene climate instability, *Paleoceanography*, *16*(1), 112–131.

Kohfeld, K. E., S. P. Harrison, C. Le Que, and R. F. Anderson (2005), Role of Marine Biology in Glacial-Interglacial CO2 Cycles, *Oceans*, *308*(2005), 74–78, doi:10.1126/science.1105375.

Large, W. G., and S. G. Yeager (2008), The global climatology of an interannually varying air–sea flux data set, *Clim. Dyn.*, *33*(2–3), 341–364, doi:10.1007/s00382-008-0441-3.

Lézine, A. M., J. C. Duplessy, and J. P. Cazet (2005), West African monsoon variability during the last deglaciation and the Holocene: Evidence from fresh water algae, pollen and isotope data from core KW31, Gulf of Guinea, *Palaeogeogr. Palaeoclimatol. Palaeoecol.*, *219*(3–4), 225–237, doi:10.1016/j.palaeo.2004.12.027.

Liu, Z. et al. (2009), Transient simulation of last deglaciation with a new mechanism for Bolling-Allerod warming., *Science*, *325*(5938), 310–4, doi:10.1126/science.1171041.

Lumpkin, R., and K. Speer (2003), Large-scale vertical and horizontal circulation in the North Atlantic Ocean, *J. Phys. Oceanogr.*, *33*(9), 1902–1920.

Lupker, M., S. M. Aciego, B. Bourdon, J. Schwander, and T. F. Stocker (2010), Isotopic tracing (Sr, Nd, U and Hf) of continental and marine aerosols in an 18th century section of the Dye-3 ice core (Greenland), *Earth Planet. Sci. Lett.*, *295*(1–2), 277–286, doi:10.1016/j.epsl.2010.04.010.

Mahowald, N. M., A. R. Baker, G. Bergametti, N. Brooks, R. a. Duce, T. D. Jickells, N. Kubilay, J. M. Prospero, and I. Tegen (2005), Atmospheric global dust cycle and iron inputs to the ocean, *Global Biogeochem. Cycles*, *19*(4), doi:10.1029/2004GB002402.

McCreary, J. P., and P. Lu (2001), Influence of the Indonesian Throughflow on the Circulation of Pacific Intermediate Water, *J. Phys. Oceanogr.*, *31*(4), 932–942, doi:10.1175/1520-0485(2001)031<0932:IOTITO>2.0.CO;2.

McManus, J., R. Francois, and J. Gherardi (2004), Collapse and rapid resumption of Atlantic meridional circulation linked to deglacial climate changes, *Nature*, *428*(6985), 834–837.

Meckler, A. N., D. M. Sigman, K. a Gibson, R. François, A. Martínez-García, S. L. Jaccard, U. Röhl, L. C. Peterson, R. Tiedemann, and G. H. Haug (2013), Deglacial pulses of deep-ocean silicate into the subtropical North Atlantic Ocean., *Nature*, *495*(7442), 495–8, doi:10.1038/nature12006.

Nace, T. E., P. a. Baker, G. S. Dwyer, C. G. Silva, C. a. Rigsby, S. J. Burns, L. Giosan, B. Otto-Bliesner, Z. Liu, and J. Zhu (2014), The role of North Brazil Current transport in the paleoclimate of the Brazilian Nordeste margin and paleoceanography of the western tropical Atlantic during the late Quaternary, *Palaeogeogr. Palaeoclimatol. Palaeoecol.*, *415*, 3–13, doi:10.1016/j.palaeo.2014.05.030.

Nurnberg, D., and R. Tiedemann (2004), Environmental change in the Sea of Okhotsk during the last 1.1 million years, *Paleoceanography*, *19*(4), 1–23, doi:10.1029/2004PA001023.

Osborne, A. H., B. A. Haley, E. C. Hathorne, S. Flögel, and M. Frank (2014), Neodymium isotopes and concentrations in Caribbean seawater: Tracing water mass mixing and continental input in a semi-enclosed ocean basin, *Earth Planet. Sci. Lett.*, *406*, 174–186, doi:10.1016/j.epsl.2014.09.011.

Pahnke, K., S. L. Goldstein, and S. R. Hemming (2008), Abrupt changes in Antarctic Intermediate Water circulation over the past, *Nat. Geosci.*, *1*(12), 870–874, doi:10.1038/ngeo360.

Palter, J. B., and M. S. Lozier (2008), On the source of Gulf Stream nutrients, *J. Geophys. Res.*, *113*(C6), C06018, doi:10.1029/2007JC004611.

Pena, L. D., S. L. Goldstein, S. R. Hemming, K. M. Jones, E. Calvo, C. Pelejero, and I. Cacho (2013), Rapid changes in meridional advection of Southern Ocean intermediate waters to the tropical Pacific during the last 30kyr, *Earth Planet. Sci. Lett.*, *368*, 20–32, doi:10.1016/j.epsl.2013.02.028.

Rempfer, J., T. F. Stocker, F. Joos, J.-C. Dutay, and M. Siddall (2011), Modelling Nd-isotopes with a coarse resolution ocean circulation model: Sensitivities to model parameters and source/sink distributions, *Geochim. Cosmochim. Acta*, *75*(20), 5927–5950, doi:10.1016/j.gca.2011.07.044.

Rempfer, J., T. F. Stocker, F. Joos, and J.-C. Dutay (2012a), On the relationship between Nd isotopic composition and ocean overturning circulation in idealized freshwater discharge events, *Paleoceanography*, *27*(3), doi:10.1029/2012PA002312.

Rempfer, J., T. F. Stocker, F. Joos, and J.-C. Dutay (2012b), Sensitivity of Nd isotopic composition in seawater to changes in Nd sources and paleoceanographic implications, *J. Geophys. Res.*, *117*(C12), C12010, doi:10.1029/2012JC008161.

Resplandy, L., L. Bopp, J. C. Orr, and J. P. Dunne (2013), Role of mode and intermediate waters in future ocean acidification: Analysis of CMIP5 models, *Geophys. Res. Lett.*, *40*(12), 3091–3095, doi:10.1002/grl.50414.

Rickaby, R. E. M., and H. Elderfield (2005), Evidence from the high-latitude North Atlantic for variations in Antarctic Intermediate water flow during the last deglaciation, *Geochemistry, Geophys. Geosystems*, *6*(5), doi:10.1029/2004GC000858.

Rickli, J., M. Frank, A. R. Baker, S. Aciego, G. de Souza, R. B. Georg, and A. N. Halliday (2010), Hafnium and neodymium isotopes in surface waters of the eastern Atlantic Ocean: Implications for sources and inputs of trace metals to the ocean, *Geochim. Cosmochim. Acta*, *74*(2), 540–557, doi:10.1016/j.gca.2009.10.006.

Rincon-Martinez, D., F. Lamy, S. Contreras, G. Leduc, E. Bard, C. Saukel, T. Blanz, A. MacKensen, and R. Tiedemann (2010), More humid interglacials in Ecuador during the past 500 kyr linked to latitudinal shifts of the equatorial front and the Intertropical Convergence Zone in the eastern tropical Pacific, *Paleoceanography*, *25*(2), 1–15, doi:10.1029/2009PA001868.

Rintoul, S. R. (1991), South Atlantic interbasin exchange, *J. Geophys. Res.*, *96*(C2), 2675, doi:10.1029/90JC02422.

Rühs, S., and K. Getzlaff (2015), On the suitability of North Brazil Current transport estimates for monitoring basin-scale AMOC changes, *Geophys. Res. Lett.*, 8072–8080, doi:10.1002/2015GL065695.Received.

Sabine, C. L. (2004), The Oceanic Sink for Anthropogenic CO2, *Science (80-.).*, *305*(5682), 367–371, doi:10.1126/science.1097403.

Saenko, O., A. Weaver, and J. Gregory (2003), On the link between the two modes of the ocean thermohaline circulation and the formation of global-scale water masses, *J. Clim.*, *16*(17), 2797–2801.

Sarmiento, J. L., N. Gruber, M. A. Brzezinski, and J. P. Dunne (2004), High-latitude controls of thermocline nutrients and low latitude biological productivity., *Nature*, *427*(6969), 56–60, doi:10.1038/nature10605.

Schmid, C., G. Siedler, and W. Zenk (2000), Dynamics of Intermediate Water Circulation in the Subtropical South Atlantic, *J. Phys. Oceanogr.*, 3191–3211.

Schmitz, W., and M. McCartney (1993), On the north Atlantic circulation, *Rev. Geophys.*, (92), 29–49.

Stoll, H. M., D. Vance, and A. Arevalos (2007), Records of the Nd isotope composition of seawater from the Bay of Bengal: Implications for the impact of Northern Hemisphere cooling on ITCZ movement, *Earth Planet. Sci. Lett.*, *255*(1–2), 213–228, doi:10.1016/j.epsl.2006.12.016.

Stouffer, R., D. Seidov, and B. Haupt (2007), Climate response to external sources of freshwater: North Atlantic versus the Southern Ocean, *J. Clim.*, *30*(3), 436–448.

Tachikawa, K., V. Athias, and C. Jeandel (2003), Neodymium budget in the modern ocean and paleo-oceanographic implications, *J. Geophys. Res.*, *108*(C8), 3254, doi:10.1029/1999JC000285.

Talley, L. (1996), *Antarctic Intermediate Water in the South Atlantic*.

Toggweiler, J. R., and B. Samuels (1995), Effect of drake passage on the global thermohaline circulation, *Deep. Res. Part I*, *42*(4), 477–500, doi:10.1016/0967-0637(95)00012-U.

Tütken, T., A. Eisenhauer, B. Wiegand, and B. T. Hansen (2002), Glacial-interglacial cycles in Sr and Nd isotopic composition of Arctic marine sediments triggered by the Svalbard/Barents Sea ice sheet, *Mar. Geol.*, *182*(3–4), 351–372, doi:10.1016/S0025-3227(01)00248-1.

Vallis, G. (2000), Large-scale circulation and production of stratification: Effects of wind, geometry, and diffusion, *J. Phys. Oceanogr.*, (1962), 933–954.

Wainer, I., M. Goes, L. N. Murphy, and E. Brady (2012), Changes in the intermediate water mass formation rates in the global ocean for the Last Glacial Maximum, mid-Holocene and pre-industrial climates, *Paleoceanography*, *27*(3), n/a-n/a, doi:10.1029/2012PA002290.

Weaver, A. J., O. A. Saenko, P. U. Clark, and J. X. Mitrovica (2003), Meltwater pulse 1A from Antarctica as a trigger of the Bølling-Allerød warm interval., *Science (80-.).*, *299*(5613), 1709–13, doi:10.1126/science.1081002.

Wolfe, C. L., and P. Cessi (2010), What Sets the Strength of the Middepth Stratification and Overturning Circulation in Eddying Ocean Models?, *J. Phys. Oceanogr.*, *40*(7), 1520–1538, doi:10.1175/2010JPO4393.1.

Wolff, E. W. et al. (2006), Southern Ocean sea-ice extent, productivity and iron flux over the past eight glacial cycles., *Nature*, *440*(7083), 491–496, doi:10.1038/nature06271.

Xie, R. C., F. Marcantonio, and M. W. Schmidt (2012), Deglacial variability of Antarctic Intermediate Water penetration into the North Atlantic from authigenic neodymium isotope ratios, *Paleoceanography*, *27*(3), doi:10.1029/2012PA002337.

Zahn, R., and A. Stüber (2002), Suborbital intermediate water variability inferred from paired benthic foraminiferal Cd/Ca and δ 13 C in the tropical West Atlantic and linking with North Atlantic, *Earth Planet. Sci. Lett.*, *200*, 191–205.

Zektser, I. S., and H. A. Loaiciga (1993), Groundwater fluxes in the global hydrologic cycle: past, present and future, *J. Hydrol.*, *144*(1–4), 405–427, doi:10.1016/0022-1694(93)90182-9.

Zhang, D., R. Msadek, M. J. McPhaden, and T. Delworth (2011), Multidecadal variability of the North Brazil Current and its connection to the Atlantic meridional overturning circulation, *J. Geophys. Res.*, *116*(C4), C04012, doi:10.1029/2010JC006812.

Zhang, J. (2016), Understanding the deglacial evolution of deep Atlantic water masses in an isotope-enabled ocean model.

Figures

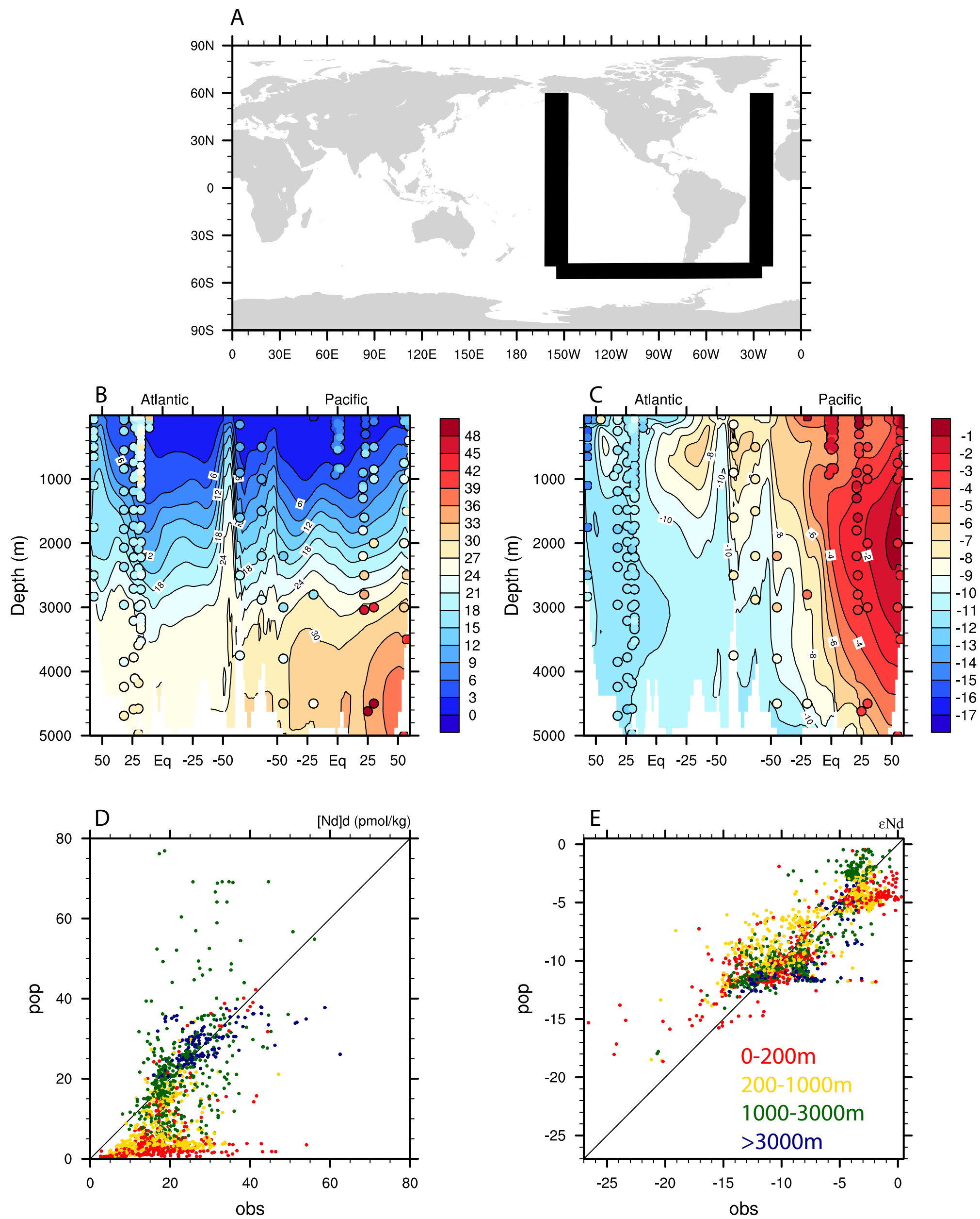

Figure.1 Model-data comparison of Nd concentration and ε_{Nd}. (A) Location of a track from the North Atlantic to the North Pacific: 20°W-30°W in the Atlantic, 54°S-56°S in the Southern Ocean and 150°W-160°W in the Pacific. (B) Nd concentration (pmol/kg)($[Nd]_d$) along the track. (C) ε_{Nd} along the track. Color contours are model results and observations are attached as filled cycles using the same color map in B and C. (D) Scatter plot of model and observational Nd concentration. (E) Scatter plot of model ε_{Nd} and observational ε_{Nd}. Colors in D and E indicated different depth range: 0-200m (red), 200m-1000m (yellow), 1000m-3000m (green) and deeper than 3000m (blue).

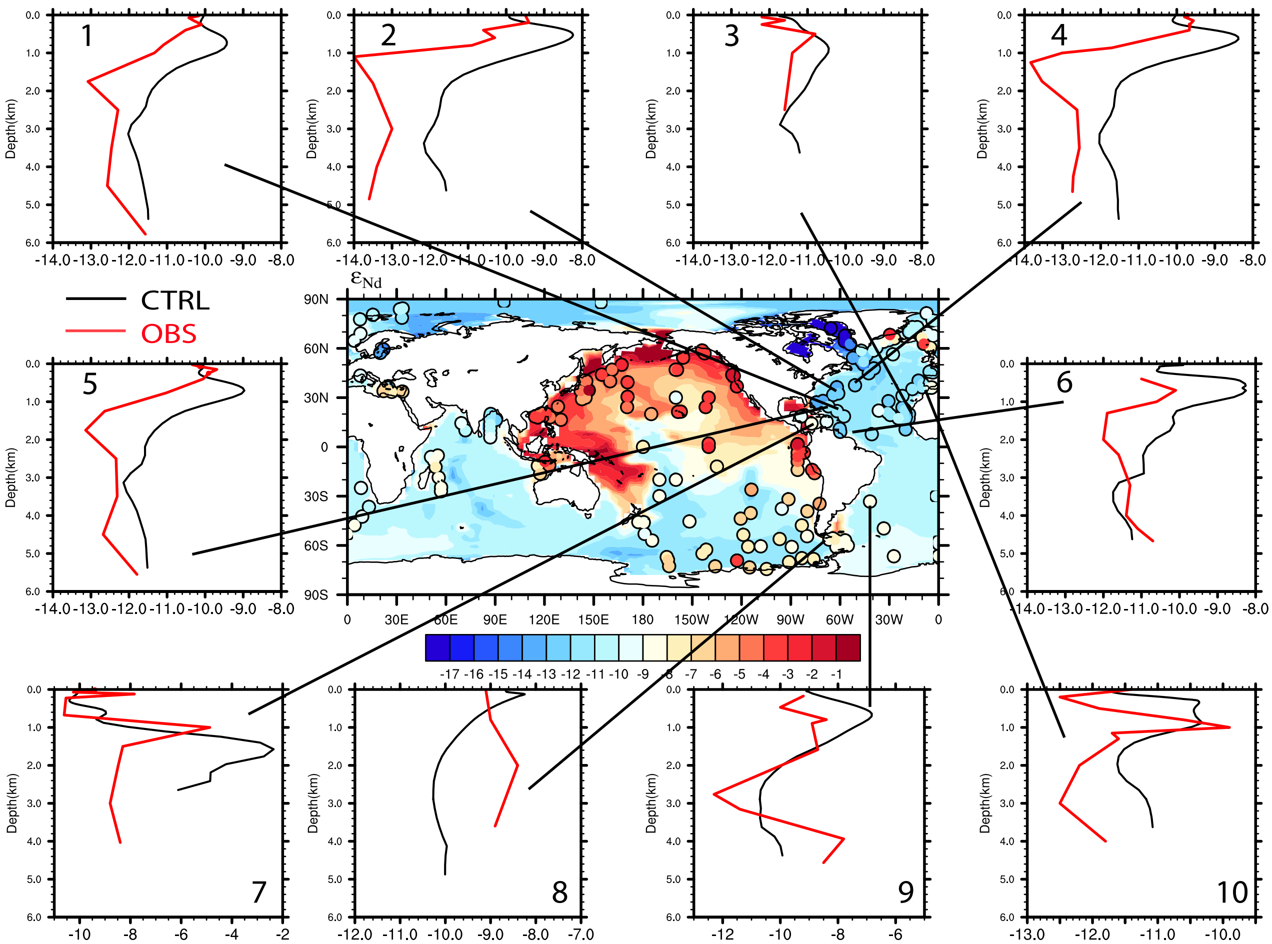

Figure 2. Comparison of ε_{Nd} fields between model and observation. (A) Global map of ε_{Nd} at the sea floor from the equilibrium state in CTRL. Observations [*van de Flierdt et al.*, 2016] are superimposed as filled circles, using the same color scale. Selected vertical profiles, focusing on tropical Atlanitc, show observed (red) and simulated (black) ε_{Nd} values.

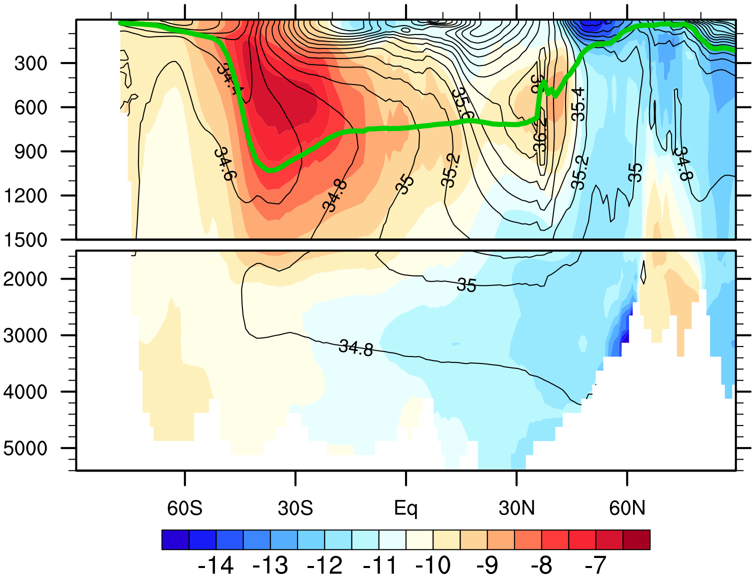

Fig.3 Atlantic zonal mean ε_{Nd} (color shading) and salinity (black contour) from CTRL. The green line is the isopycal line of σ_{AAIW}.

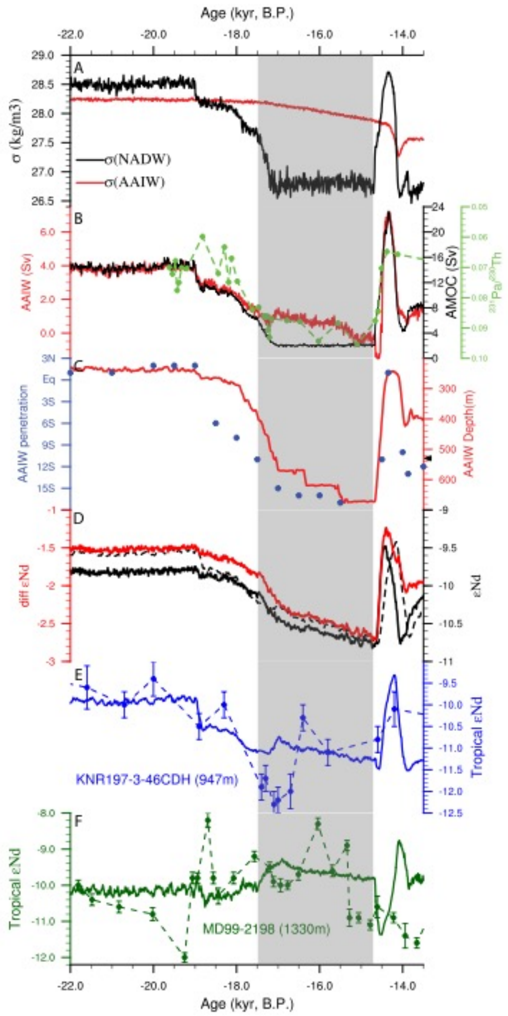

Fig.4: Evolution during the last deglaciation in reconstructions and iPOP2-TRACE. (A) Winter surface density in NADW (black) and AAIW (red) production region. (B) Model maximum AMOC transport (under 500m) in iPOP2-TRACE (black), Sedimentary $^{231}Pa/^{230}Th$ record of OCE326-5GGC [*McManus et al.*, 2004] (dashed green) and AAIW transport which is defined as the meridional transport at equatorial Atlantic of layers between (σ_{AAIW} -0.5) and (σ_{AAIW} +0.5) (red). (C) Estimation of AAIW northward penetration latitude (navy dots). AAIW depth at equatorial Atlantic (red). Black triangle on the right of Y axis indicates the late Holocene AAIW depth. (D) Zonal mean AAIW ε_{Nd} value at equatorial Atlantic (solid black), the difference between AAIW ε_{Nd} value at equatorial Atlantic and AAIW end-member ε_{Nd} value (red) and ε_{Nd} value at 1,000 m at western boundary equatorial Atlantic (dashed black). (E) ε_{Nd} reconstruction in Demerara Rise (dashed navy) and ε_{Nd} evolution at this location in iPOP2-TRACE (solid navy). (F) ε_{Nd} records from Tobago Basin (dashed green) and ε_{Nd} evolution at this location in iPOP2-TRACE (solid green). HS1 is indicated by grey shading.

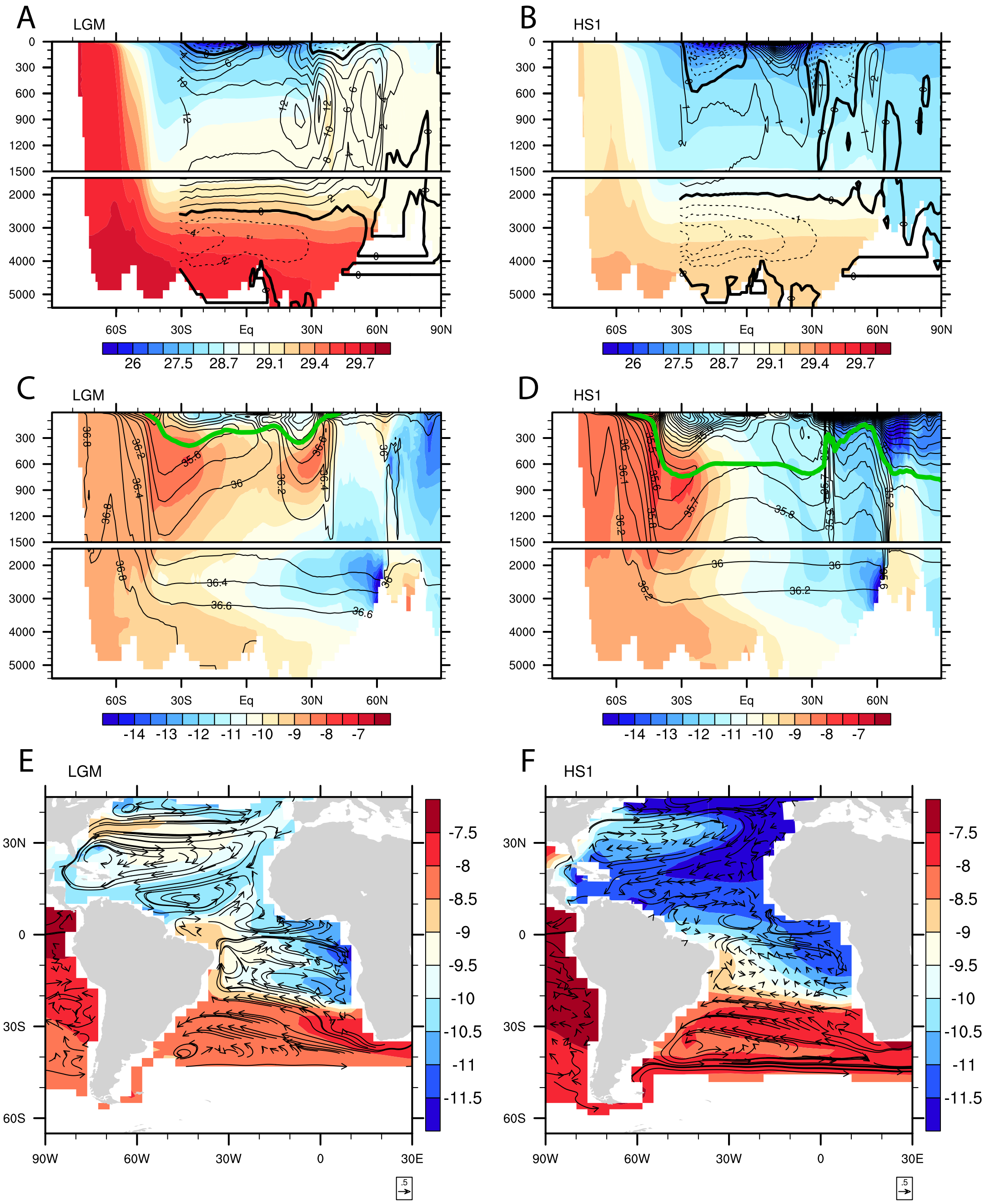

Fig.5: Comparison between LGM (20 kyr B.P.) and HS1 (16 kyr B.P.) in iPOP2-TRACE experiment. Atlantic overturning streamfunction (black contour) and Atlantic zonal mean potential density (color shading) during (A) LGM and (B) HS1. Atlantic zonal mean ε_{Nd} (color shading), salinity (black contour) and isopycnal line for σ_{AAIW} (green line) at (C) LGM and (D) HS1. Circulation (vectors) and ε_{Nd} (color) at σ_{AAIW} surface: (E) LGM and (F) HS1.

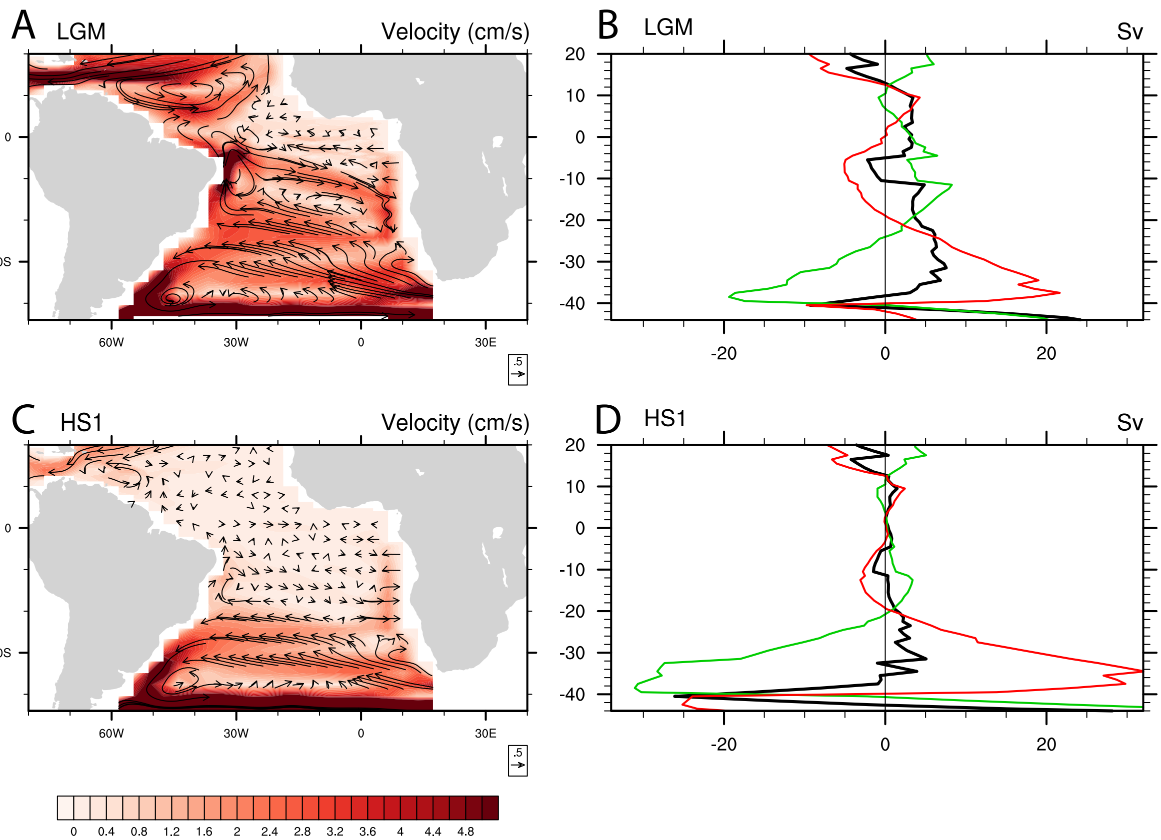

Fig.6 Velocity and meridional transport at annual mean σ_{AAIW} surface during LGM and HS1. (A) Vectors indicate direction and magnitude of (u,v) (cm/s) and color indicate magnitude (cm/s) during LGM. (B) meridional transport (Sv) at different latitudes during LGM, green for western boundary transport, red for interior and black for total transport. Same for (C) and (D) during HS1.

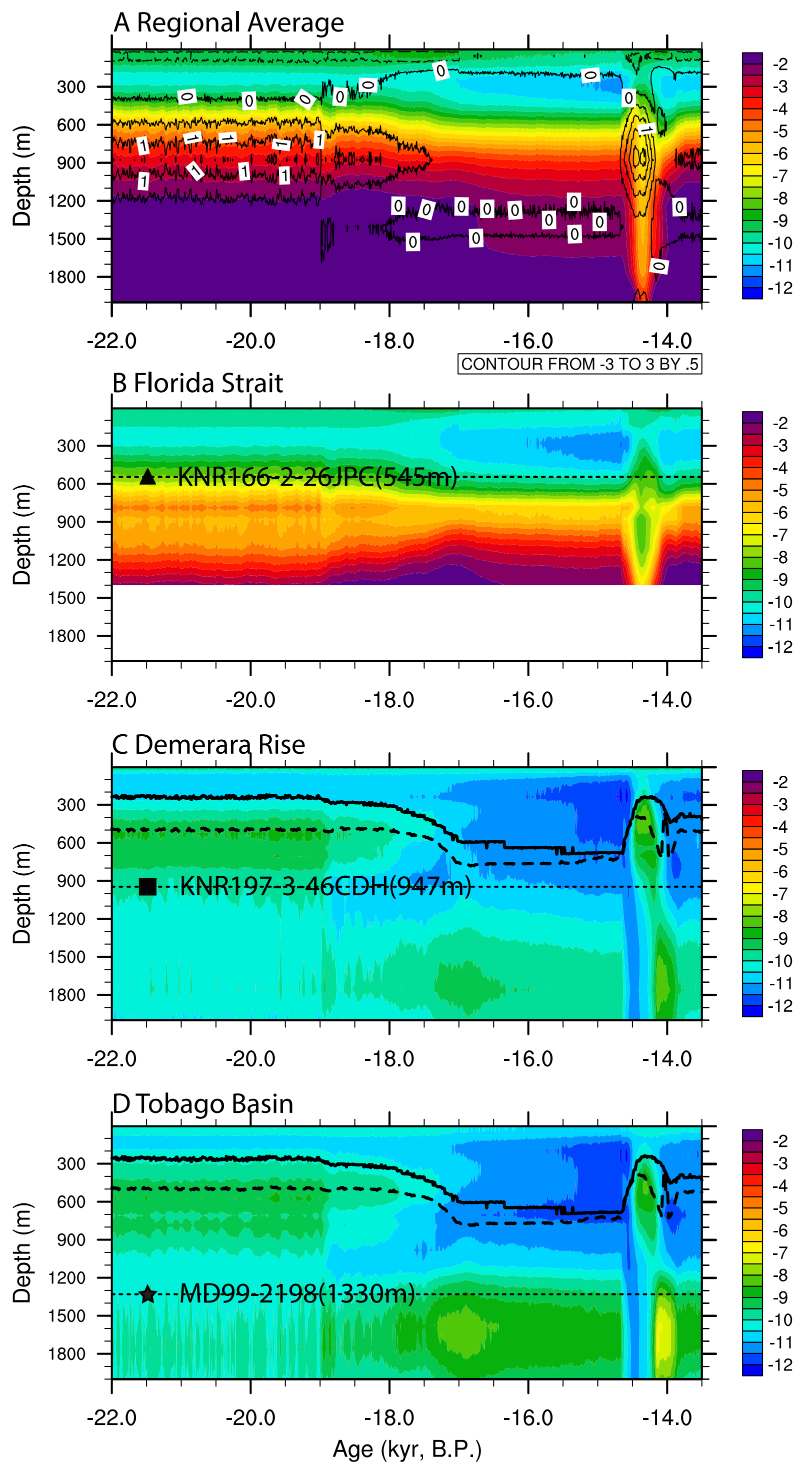

820
821 Fig.7: ε_{Nd} evolution for the upper 2,000m at four different locations in the tropical North Atlantic sites.
822 (A) Area average from Gulf of Mexico and Caribbean Sea (15°N-30°N, 85°W-100°W). Black contours
823 are vertical velocity in 10^{-4} cm/s. (B) (24.33°N, 83.25°W), which is the horizontal location for site

KNR166-2-26JPC in Florida Strait (C) (7.84°N, 53.66°W), which is the horizontal location for site KNR197-3-46CDH in Demerara Rise and (D) (12.09°N,61.23°W), which is the horizontal location for site MD99-2198 in Tobago Basin. The depth of each core is indicated by a thin black dash line with filled symbol: KNR166-2-26JPC(triangle), KNR197-3-46CDH (square) and MD99-2198 (star). The depth of σ_{AAIW} is indicated by thick black lines in C and D: σ_{AAIW} by salinity (solid, defined in text) and σ_{AAIW} by ε_{Nd} (dash, defined as average of potential density where ε_{Nd} reaches maximum vertically Atlantic average from 40°S to equator). The maximum ε_{Nd} tongue is shifted slightly deeper in the minimum salinity tongue, because of the reversible scavenging by settling particles [*Rempfer et al.*, 2011].

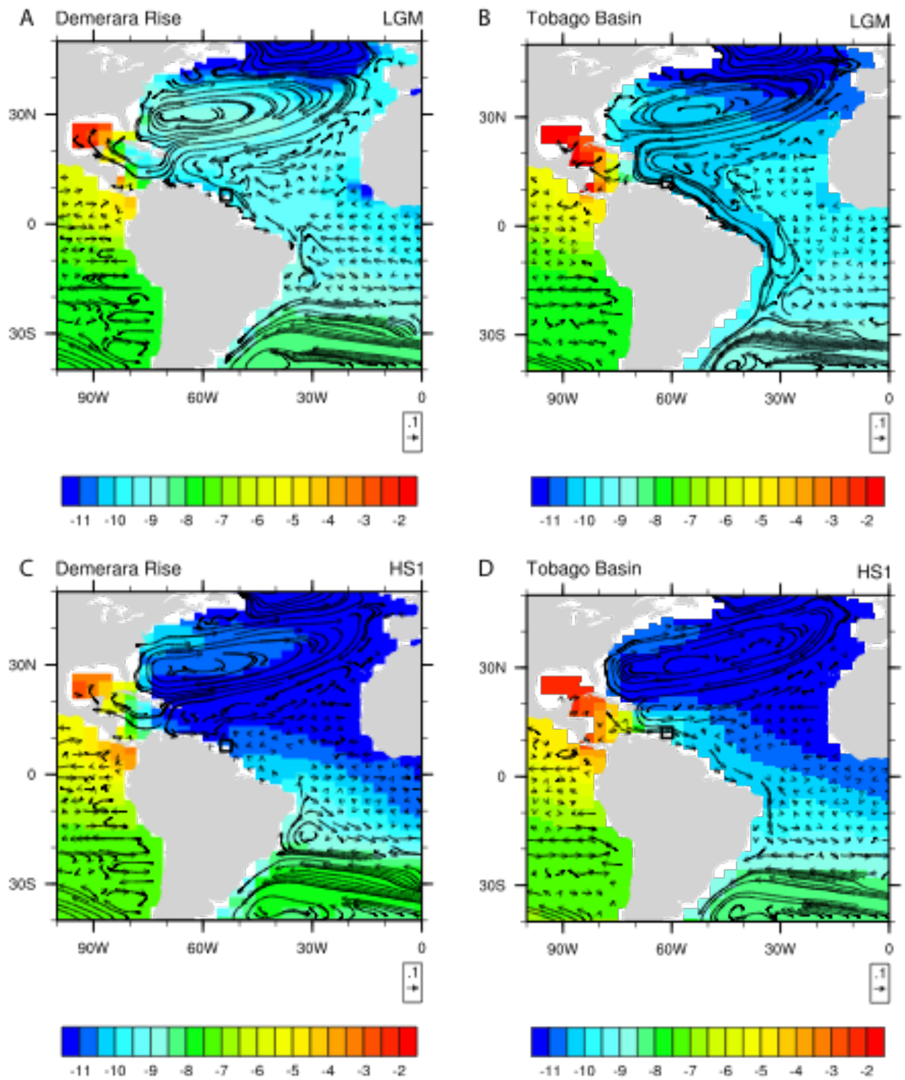

Fig. 8 Ocean current (vector) and ε_{Nd} (color) at the depth of KNR197-3-46CDH (947m) (A and C) and MD99-2198 (1330m) (B and D) during LGM and HS1. The location of each site is indicated by a black box.

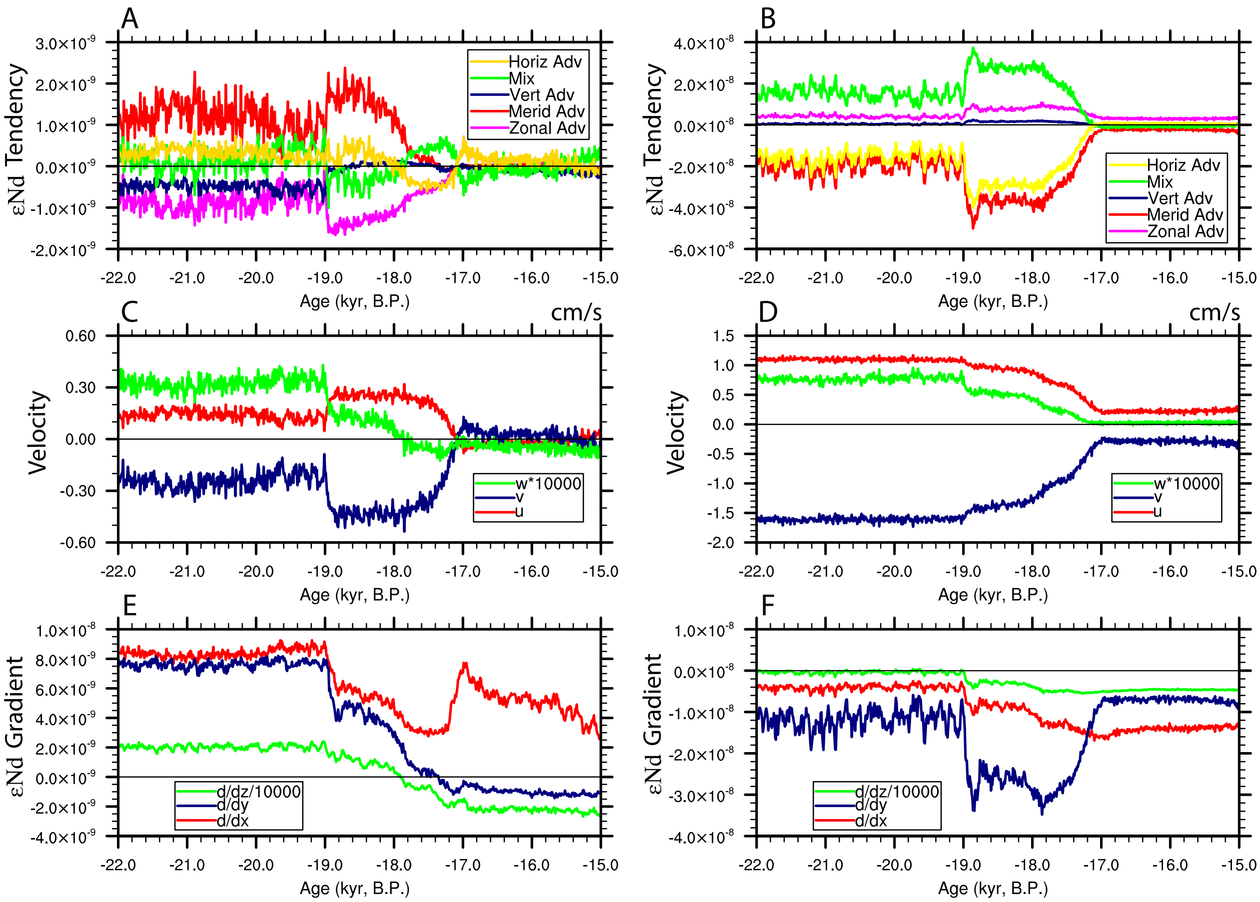

Fig.9 ε_{Nd} tracer budget analysis for site KNR197-3-46CDH (A, C and E) and MD99-2198 (B, D and F). A and B, time series of ε_{Nd} tendency terms: zonal advection (magenta), meridional advection (red), horizontal advection (zonal advection + meridional advection) (yellow), vertical advection (navy) and mixing (green). C and D, evolution of velocity: zonal velocity (u) (red), meridional velocity (v) (navy) and vertical velocity multiplied by 10^4 (w) (green). E and F, ε_{Nd} gradient: zonal gradient (red), meridional gradient (navy) and vertical gradient (green).

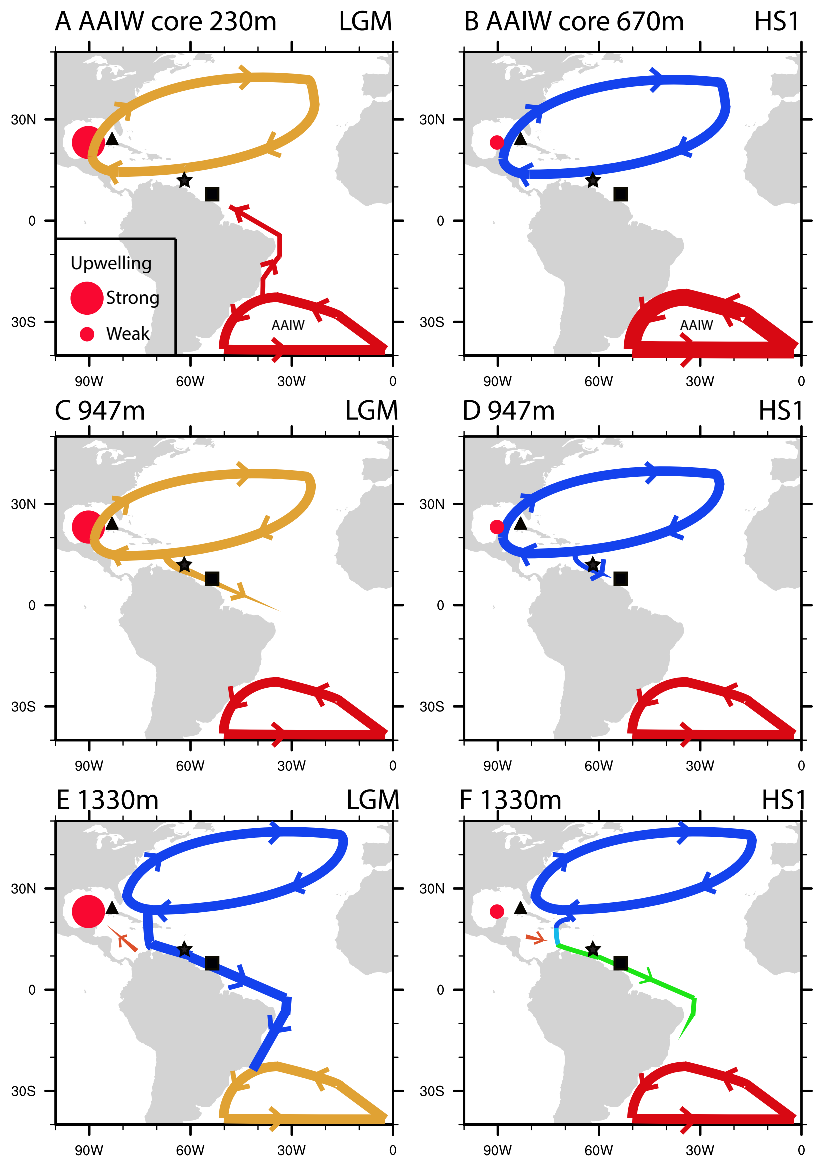

Fig.10 Schematic figure of circulation and $\boldsymbol{\varepsilon_{Nd}}$ during LGM and HS1 at different depth: AAIW core depth (A and B), 947 m (C and D) and 1330 m (E and F). Red filled circle represents upwelling in the Gulf of Mexico and Caribbean Sea, with larger size for stronger upwelling. Curves with arrows represents flow, with thickness for flow magnitude and color from blue to green to yellow to red for the increasing of ε_{Nd}. Locations of each observational site are indicated by filled symbols: KNR166-2-26JPC: (24°19.62'N, 83°15.14'W, 546m), triangle; MD99-2198: (12.09°N, 61.23°W, 1330m), star; KNR197-3-46CDH: (7.836°N, 53.663°W, 947m), square.